Journal of Science and Technology in Civil Engineering, NUCE 2021. 15 (2): 77–89

A BUBBLE-ENHANCED QUADRILATERAL FINITE ELEMENT FOR ESTIMATION BEARING CAPACITY FACTORS OF STRIP FOOTING

Vo Minh Thien[a,*]

[a]*Faculty of Civil Engineering, Ho Chi Minh City University of Technology (HUTECH), 475A Dien Bien Phu street, Binh Thanh district, Ho Chi Minh city, Vietnam*

Article history:
Received 21/12/2020, Revised 04/03/2021, Accepted 29/03/2021

Abstract

In this paper, a computational approach using a combination of the upper bound theorem and the bubble-enhanced quadrilateral finite element (FEM-Qi6) is proposed to evaluate bearing capacity factors of strip footing in cohesive-frictional soil. The new element is built based on the quadrilateral element (Q4) by adding a pair of internal nodes to solve the volumetric locking phenomenon. In the upper bound finite element limit analysis, the soil behaviour is described as a perfectly plastic material and obeys associated plastic flow rule following the Mohr-Coulomb failure criterion. The discrete limit analysis problem can be formulated in the form of the well-known second-order cone programming to utilize the interior-point method efficiently. The bearing capacity factors of strip footing and failure mechanisms in both rough and smooth interfaces are obtained directly from solving the optimization problems and presented in design tables and charts for engineers to use. To demonstrate the accuracy of the proposed method, the results of bearing capacity factors using FEM-Qi6 were compared with those available in the literature.

Keywords: limit analysis; bearing capacity factors; strip footing; SOCP; FEM-Qi6.

https://doi.org/10.31814/stce.nuce2021-15(2)-07

1. Introduction

The bearing capacity of a shallow strip footing is generally determined by using the following Terzaghi [1] equation:

$$q_u = cN_c + qN_q + \frac{1}{2}\gamma BN_\gamma \tag{1}$$

where N_c, N_q, N_γ are three bearing capacity factors related to the cohesion c, the surcharge load q and the unit weight of the soil γ, respectively.

Analytical expressions N_c, N_q are given by Prandtl [2] and Reissner [3] for a strip footing on weightless soil while the exact values N_γ remain unknown. In 1943, Terzaghi [1] proposed a bearing capacity equation to calculate N_γ the factor for strip footing with a rough base using a limit equilibrium method. Meyerhof [4] used the Prandtl failure mechanism to evaluate the bearing capacity factor N_γ for strip footing with a rough base.

In a few past decades, Sokolovskii [5] estimated the bearing capacity factor N_γ using the slip-line method. Hansen [6] used quasi-empirical modifications of a slip-line solution for the bearing

*Corresponding author. *E-mail address:* vm.thien@hutech.edu.vn (Thien, V. M.)

capacity of shallow foundation and proposed an expression for N_γ. Vesic [7] evaluated the bearing capacity factor N_γ based on Prandtl's mechanism and numerical studies suggested by Caquot and Kreisel [8]. Bolton and Lau [9] used a method of characteristic with the Mohr-Coulomb criterion to evaluate the bearing capacity of circular and strip footings with rough and smooth bases.

Some decades ago, the finite element method (FEM) had been rapidly developing to solve complicated geotechnical problems. In the study of Griffiths [10], the soil was presented by an elastoplastic model with a Mohr-Coulomb yield condition, in conjunction with a non-associated flow rule (zero plastic volume change). Due to numerical convergence problems, Griffiths investigated cases where friction angles $\phi \leq 35^\circ$. Frydman and Burd [11] carried out numerical studies to evaluate bearing capacity factor N_γ for linear elastic perfectly plastic soil material using finite element and finite difference methods. Ukrichon et al. [12] performed an upper bound and lower bound limit analysis using linear programming and finite element method to calculate the bearing capacity factor N_γ. Hjiaj et al. [13] applied nonlinear programming using the finite element to evaluate the self-weight bearing capacity factor N_γ for smooth and rough footing. Martin [14] used stress characteristics to calculate high-precision N_γ factors for both smooth and rough footings. Recently, Makrodimopoulous and Martin [15] using 6 node-triangular element and second-order cone programming to calculate the bearing capacity factor N_γ for both smooth and rough footings. By employing the upper limit analysis, T. Vo-Minh [16] estimated bearing capacity factors of strip footing using the node-based smoothed finite element method and second-order cone programming.

The standard finite element method using the 3-node triangular element (T3) or 4-node quadrilateral element (Q4) is popular due to its simplicity. One of the significant drawbacks of low-order elements (T3 and Q4) is the volumetric locking phenomenon, which often occurs in nearly incompressible materials. To overcome disadvantages, many methods were suggested to reduce integration methods [17], enhanced assumed strain [18–20], an average nodal technique [21], a mesh-free method based on the radial basis function [22] and so on. In recent years, H. Nguyen-Xuan et al. [23, 24] researched the enrich-bubble 3-node triangular element (T3) combined with an edge-based smoothing technique to solve the limit analysis of structures. More recently, T. Vu-Hoang et al. [25] used the FEM-Qi6 to evaluate the elastoplastic nonlinear analysis of strip footings and slope stability.

In this paper, a bubble-enhanced quadrilateral element (FEM-Qi6) is proposed to evaluate strip footing bearing capacity factors using upper bound limit analysis. The new element is built based on the quadrilateral element (Q4) by adding a pair of internal nodes to solve the locking mode. This method's concept uses a bubble function to enhance the compatible strain, and an extra field of variables related to the space derivatives of the displacement field is added. Internal plastic dissipation is minimized in the upper bound limit analysis to determine the soil's ultimate load-bearing capacity. The Mohr-Coulomb yield criterion can be formed in a second-order cone programming (SOCP). To solve the resulting conic problems, the MATLAB (version 7.8.0) and the Mosek (version 6.0) [26] are used to give all solutions in this paper.

2. Brief on the bubble-enhanced quadrilateral element (FEM-Qi6)

Lower order elements (T3 and Q4) have been proved to suffer volumetric locking. This phenomenon has been encountered in the analysis of undrained (incompressible) problems, where the elements do not provide enough degrees of freedom to satisfy the constant-volume condition (Nagtegaal, et al. [27]).

In this study, the new element is built based on the formulation of the four-node quadrilateral element (Q4) by adding two extra compatible modes of deformation in the definition of the displace-

ment field. In the literature, the implementation of bubble function stems from overly stiff properties of Q4 elements where four edges remain straight when deformation occurs. In compensation for the overly stiff behaviour, bubble functions accounted for the internal deformation are introduced. This method belongs to the branch of the mixed formulation [28–30]. The mixed formulation leads to the violation of compatible conditions of FEM [31]. The F-bar method [32] has been extensively applied for both small and large strain plasticity analysis. In the present approach, the same framework of a mixed formulation is applied, but compatible conditions are preserved. If the displacement field is only defined from the standard expansion in terms of bilinear shape functions, the divergence of the displacement field is never equal to zero at the Gauss points, as shown in Fig. 1.

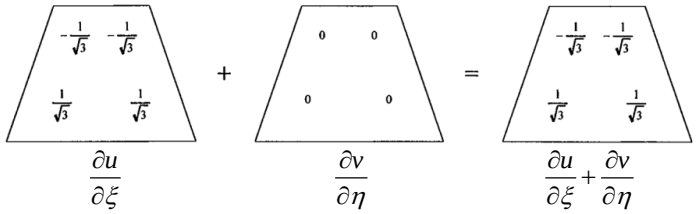

Figure 1. Locking test at the Gauss points of the b_6 mode of deformation with full integration

An extra compatible displacement field $\mathbf{u}_\alpha^h$ is introduced into the finite element method displacement field as shown in Fig. 2.

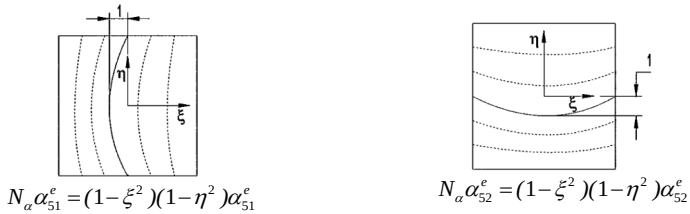

Figure 2. Additional compatible modes

$$\mathbf{u}^h = \mathbf{u}_d^h + \mathbf{u}_\alpha^h = \sum_{i=1}^{4} N_i(\xi,\eta)\mathbf{d_i^e} + N_\alpha(\xi,\eta)\alpha^e \tag{2}$$

$$\mathbf{d_i^e} = \begin{bmatrix} u_i^e \\ v_i^e \end{bmatrix}, \quad \alpha^e = \begin{bmatrix} \alpha_{51}^e \\ \alpha_{52}^e \end{bmatrix} \tag{3}$$

$$N_\alpha = (1-\xi^2)(1-\eta^2) \tag{4}$$

The extra displacement field is related to the internal movement of the element, which has zero values at the element boundary. The values α^e are the internal variables that may be associated with the displacement of the central point. It is advisable not to consider the contribution of these additional fields in the evaluation of body forces.

$$\frac{\partial u_\alpha}{\partial \xi}\alpha_{51}^e + \frac{\partial v_\alpha}{\partial \eta}\alpha_{52}^e = -2\xi(1-\eta^2)\alpha_{51}^e - 2\eta(1-\xi^2)\alpha_{52}^e \tag{5}$$

In the locking test of Fig. 1, if we implement the following values to the new variables, $\nabla \mathbf{u}^h = 0$ at the Gauss points, as illustrated in Fig. 3.

$$\alpha_{51}^e = 0, \quad \alpha_{52}^e = -\frac{3}{4} \tag{6}$$

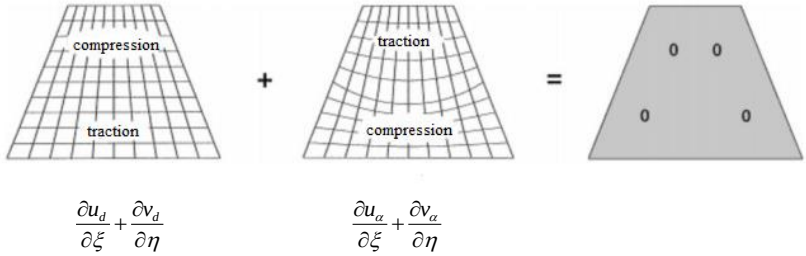

Figure 3. Locking test with additional compatible modes

Next, the strain field can be defined

$$\boldsymbol{\varepsilon} = \boldsymbol{\varepsilon}_d + \boldsymbol{\varepsilon}_\alpha = \underbrace{\begin{bmatrix} \mathbf{B}_d^e & \mathbf{B}_\alpha^e \end{bmatrix}}_{\mathbf{B}} \underbrace{\begin{bmatrix} \mathbf{d}^e \\ \alpha^e \end{bmatrix}}_{\mathbf{d}} \tag{7}$$

where

$$\mathbf{B}_d^e = \begin{bmatrix} \dfrac{\partial N_I}{\partial x} & \\ & \dfrac{\partial N_I}{\partial y} \\ \dfrac{\partial N_I}{\partial y} & \dfrac{\partial N_I}{\partial x} \end{bmatrix}_{I=1,2,3,4} \tag{8}$$

$$\mathbf{B}_\alpha^e = \begin{bmatrix} \dfrac{\partial N_\alpha}{\partial x} & 0 & 0 & 0 \\ 0 & \dfrac{\partial N_\alpha}{\partial y} & 0 & 0 \\ 0 & 0 & \dfrac{\partial N_\alpha}{\partial y} & \dfrac{\partial N_\alpha}{\partial x} \end{bmatrix} \tag{9}$$

It is easy to examine that

$$\int_\Omega \mathbf{B}_\alpha^e \mathrm{d}\Omega = \int_{-1}^{1}\int_{-1}^{1} \mathbf{B}_\alpha^e \, \|J\| \, \mathrm{d}\xi \mathrm{d}\eta = 0 \tag{10}$$

where $\mathbf{J}$ is the Jacobian matrix.

The above feature means that the additional strains do not affect patch test conditions to convergence numerical solutions. The extra variables are eliminated in the assembling process by a substructuring technique, as in the enhanced assumed strain method [19].

3. A FEM-Qi6 formulation for a plane strain with Mohr-Coulomb yield criterion

We consider a two-dimensional problem domain Ω bounded by a continuous boundary $\Gamma_{\dot{\mathbf{u}}} \cup \Gamma_{\mathbf{t}} = \Gamma, \Gamma_{\dot{\mathbf{u}}} \cap \Gamma_{\mathbf{t}} = \varnothing$. The rigid-perfectly plastic body is subjected to body forces $\mathbf{f}$ and external tractions $\mathbf{g}$ on $\Gamma_{\mathbf{t}}$ and the boundary $\Gamma_{\dot{\mathbf{u}}}$ prescribed by the displacement velocity vector $\dot{\mathbf{u}}$. The strain rates $\dot{\boldsymbol{\varepsilon}}$ can be expressed by relations

$$\dot{\boldsymbol{\varepsilon}} = \begin{bmatrix} \dot{\varepsilon}_{xx} & \dot{\varepsilon}_{yy} & \dot{\gamma}_{xy} \end{bmatrix}^T = \nabla \dot{\mathbf{u}} \tag{11}$$

The upper bound theorem states that there exists a kinematically admissible displacement field $\dot{\mathbf{u}} \in U$, such that

$$W_{\text{int}}(\dot{\boldsymbol{\varepsilon}}) = D(\dot{\boldsymbol{\varepsilon}}) < \alpha^+ W_{\text{ext}}(\dot{\mathbf{u}}) + W^0_{\text{ext}}(\dot{\mathbf{u}}) \tag{12}$$

where α^+ is the limit load multiplier of the load $\mathbf{g}$, $\mathbf{f}$ and $W^0_{\text{ext}}(\dot{\mathbf{u}})$ is the work of additional load $\mathbf{g}_0, \mathbf{t}_0$ not subjected to the multiplier.

Defining $C = \{\dot{\mathbf{u}} \in U | W_{\text{ext}}(\dot{\mathbf{u}}) = 1\}$, the limit analysis problem is based on the kinematical theorem to determine the collapse multiplier α^+ yielding the following optimization problem.

$$\alpha^+ = \min \int_{\Omega} D(\dot{\boldsymbol{\varepsilon}}) \mathrm{d}\Omega - W^0_{\text{ext}}(\dot{\mathbf{u}}) \tag{13}$$

$$st \begin{cases} \dot{\mathbf{u}} = 0 \quad \text{on } \Gamma_u \\ W_{\text{ext}}(\dot{\mathbf{u}}) = 1 \end{cases} \tag{14}$$

Makrodimopoulos and Martin [15] using the Mohr-Coulomb failure criterion and associated flow rule determine the power of plastic dissipation as follows

$$D(\dot{\boldsymbol{\varepsilon}}) = cA_i t_i \cos\phi \tag{15}$$

The strains field $\boldsymbol{\varepsilon}$ using FEM-Qi6 can be calculated from Eq. (7), the upper-bound limit analysis problem for the plane strain can be determined by minimizing the objective function

$$\alpha^+ = \min \left(\sum_{i=1}^{N_n} cA_i t_i \cos\phi - W^0_{ext}(\dot{\mathbf{u}}) \right) \tag{16}$$

$$st \begin{cases} \dot{u} = 0 \quad \text{on } \Gamma_u \\ W_{\text{ext}}(\dot{\mathbf{u}}) = 1 \\ \dot{\boldsymbol{\varepsilon}}_{xx} + \dot{\boldsymbol{\varepsilon}}_{yy} = t_i \sin\phi \\ \|\rho\|_i \le t_i, \quad i = 1, 2, \ldots, N_n \end{cases} \tag{17}$$

where N_n is the total number of nodes in the computational domain. The fourth constraint in Eq. (17) is a quadratic cone. In this paper, the computations were performed on a Dell Optiplex 990 (Intel Core$^{\text{TM}}$ i5, 1.6 GHz CPU, 8GB RAM) in a Window XP environment using the conic interior-point optimizer of the Mosek package [25].

4. Numerical examples

4.1. N_c and N_γ bearing capacity factors of strip footing

For a weightless soil ($c \geq 0, \phi \geq 0, \gamma = 0$) in the absence of surcharge, the bearing capacity of strip footing is given by $q_u = cN_c$ where N_c is a dimensionless bearing capacity factor that depends on ϕ. An analytical expression of N_γ can be determined by

$$N_c = \cot\phi \left[e^{\pi \tan\phi} \tan^2\left(\frac{\pi}{4} + \frac{\phi}{2}\right) - 1 \right] \tag{18}$$

The bearing capacity factor N_γ represents the effect of the soil weight ($c = 0, \phi \geq 0, \gamma > 0$) with no surcharge can be determined by

$$N_\gamma = \frac{q_u}{0.5B^2\gamma} \tag{19}$$

There is no analytical solution for N_γ, but it can be evaluated using various numerical methods. Due to symmetry, only half of the problem is considered. The soil behaviour is described as a uniform Mohr-Coulomb material with a value of cohesion c, friction angle ϕ and unit weight $\gamma = 0$. The typical finite element meshes of 4608 quadrilateral elements are employed in the numerical analysis, as shown in Fig. 4. To describe smooth or rough interface conditions between the footing and the soil, the lateral displacement of nodes in contact with the footing is freeing or fixing, respectively. The problem's size is chosen sufficiently large enough to ensure that the failure mechanism only takes place inside the considered domain.

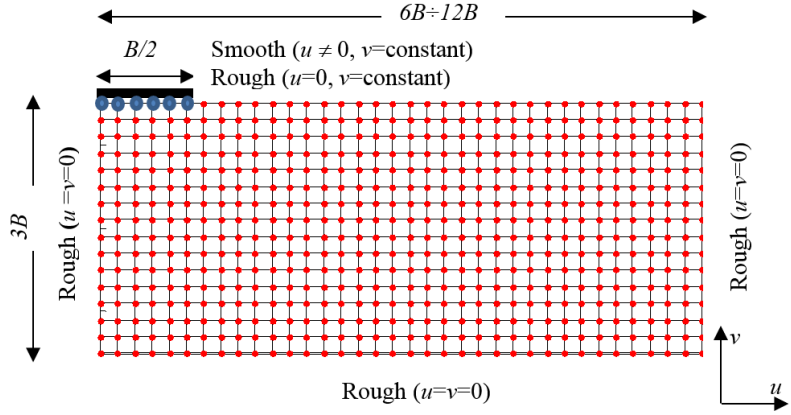

Figure 4. Typical finite element mesh of 4608 quadrilateral elements for the FEM-Qi6 model

To obtain the bearing capacity factor N_c for a weightless soil in the absence of surcharge $q = 0, c = 1, \gamma = 0, W^0_{\text{ext}}(\dot{\mathbf{u}})$ and the bearing capacity factor N_γ represent the effect of the soil weight ($c = 0, q = 0, \gamma = 1$) with no surcharge, the optimization problem for plane strain using FEM-Qi6 can be determined by

$$N_c = \alpha^+ = \min\left(\sum_{i=1}^{N_n} cA_i t_i \cos\phi - W^0_{ext}(\dot{\mathbf{u}}) \right) \tag{20}$$

$$N_\gamma = \alpha^+ = \min\left(-W^0_{\text{ext}}(\dot{\mathbf{u}}) \right) \tag{21}$$

When the soil friction angle $\phi < 30^{\circ}$,the rectangular region is $L = 6B$ and $H = 3B$, where B is the width of footing. When the soil friction angle increases $\phi \geq 30^{\circ}$, the failure mechanism expands larger in both vertical and horizontal directions, the domain size should be $L = 12B$ and $H = 5B$. Figs. 5–8 show the power dissipation of strip footing in the case of friction angle $\phi = 0^{\circ}, 10^{\circ}, 30^{\circ}, 45^{\circ}$.

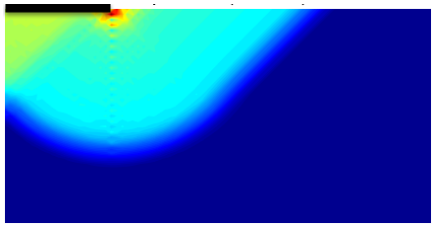

Figure 5. Power dissipation of strip footing $\phi = 0^{\circ}$

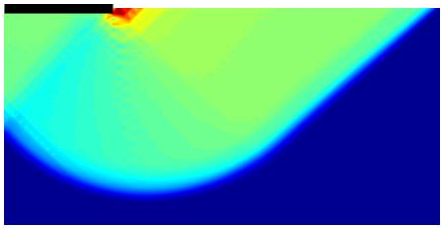

Figure 6. Power dissipation of strip footing $\phi = 10^{\circ}$

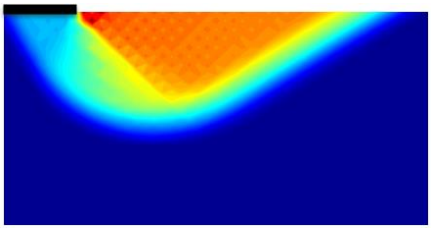

Figure 7. Power dissipation of strip footing $\phi = 30^{\circ}$

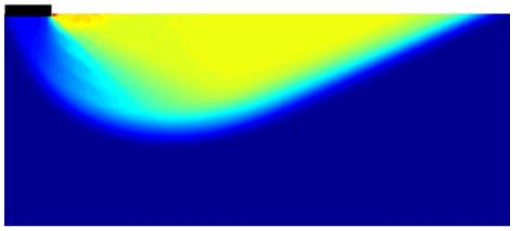

Figure 8. Power dissipation of strip footing $\phi = 45^{\circ}$

To consider the accuracy of this approach, a comparison of the bearing capacity factors of strip footing N_c, N_γ using FEM-Qi6 with those of Makrodimopoulous and Martin [15] are shown in Table 1. It is evident that the N_c factor for the case when $\phi = 35^{\circ}$ solutions obtained using 4608 quadrilateral elements (FEM-Qi6 model) agree well with the 6-node triangular element presented by Makrodimopoulous & Martin [15] using a mesh of 18719 elements, 46.38 compared with 46.37. Thus, we quickly recognize that the numerical procedure using FEM-Qi6 and SOCP reduces a significant number of elements in the optimization problem and reduces the time for solving optimization problems.

Table 1. Comparison of the bearing capacity factors of strip footingN_c, N_γ (for smooth interface)

NE	Present method (FEM-Qi6), $\phi = 35^0$		*NE*	Makrodimopoulous and Martin [15] (FEM-T6), $\phi = 35^0$	
	N_c	N_γ		N_c	N_γ
648 (Q4)	47.82	19.15	774 (T6)	49.25	19.95
1800	47.27	18.55	6308	46.99	18.14
4608	46.38	17.78	18719	46.37	17.78

NE - number of elements.

The values of the bearing capacity factor of N_c using FEM-Qi6 are summarized in Table 2 and illustrated in Fig. 9. The obtained results from the present method are very close to the analytical values of the Prandtl solution.

Table 2. Results for bearing capacity factor N_c

$\phi(^\circ)$	Terzaghi [1]	FEM-T3 (Error %)	FEM-Q4 (Error %)	FEM-Qi6 (Error %)	Exact values Prandtl [2]
5	7.34	6.621 (2.03)	6.614 (1.93)	6.614 (1.93)	6.4888
10	9.60	8.532 (2.24)	8.489 (1.72)	8.483 (1.66)	8.3449
15	12.86	11.246 (2.45)	11.132 (1.41)	11.123 (1.44)	10.9765
20	17.69	15.253 (2.82)	15.005 (1.14)	14.984 (1.00)	14.8347
25	25.13	21.571 (4.10)	20.904 (0.88)	20.952 (1.12)	20.7205
30	37.16	31.422 (4.25)	30.322 (0.60)	30.387 (0.82)	30.1396
35	57.75	47.942 (3.94)	46.542 (0.90)	46.380 (0.55)	46.1236
40	95.69	80.577 (6.99)	75.860 (0.72)	75.810 (0.66)	75.3131
45	172.29	151.841 (13.42)	138.610 (3.54)	135.277 (1.05)	133.874

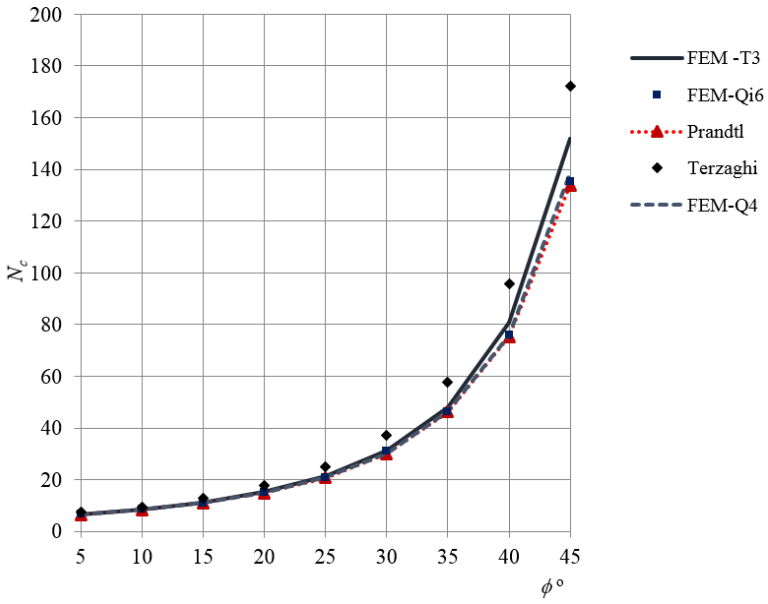

Figure 9. Comparison of N_c factors with other solutions

The computed values of bearing capacity of strip footing N_γ for friction angles $\phi = 5^\circ$ to 45° using FEM-Qi6 are summarized in Table 3. Figs. 10, 11 illustrate the comparison between N_γ using FEM-Qi6 and other solutions on a semi-log plot. It can be seen that the values of all bearing capacity factors for a rough footing are higher than those for a smooth footing base. The values of those factors obtained from the present method FEM-Qi6 are compared with the exact solution of Martin [14] by the method of stress characteristics. It demonstrates that the present method agrees well with the precise plasticity solutions.

Table 3. Results for bearing capacity factor N_γ

$\phi(^\circ)$	N_γ (FEM-Q4)		N_γ (FEM-Qi6)		Exact values N_γ [14]	
	Smooth (Error %)	Rough (Error %)	Smooth Error (%)	Rough Error (%)	Smooth	Rough
5	0.098 (16.03)	0.169 (49.02)	0.096 (13.66)	0.141 (24.33)	0.08446	0.1134
10	0.317 (12.85)	0.596 (37.58)	0.306 (8.93)	0.489 (12.88)	0.2809	0.4332
15	0.772 (10.43)	1.480 (25.31)	0.746 (6.70)	1.306 (10.58)	0.6991	1.181
20	1.713 (8.48)	3.333 (16.80)	1.658 (5.00)	2.986 (5.17)	1.579	2.839
25	3.699 (6.87)	7.310 (12.62)	3.584 (3.55)	6.597 (1.63)	3.461	6.491
30	8.068 (5.42)	16.152 (9.50)	7.828 (2.28)	14.625 (−0.85)	7.653	14.75
35	18.282 (3.99)	36.978 (7.24)	17.783 (1.15)	33.571 (−2.63)	17.58	34.48
40	44.339 (2.66)	90.514 (5.77)	43.051 (−0.32)	85.232 (−0.39)	43.19	85.57
45	118.780 (1.00)	250.356 (6.89)	115.446 (−1.83)	242.453 (3.52)	117.6	234.2

4.2. N_q bearing capacity factor of strip footing

Reissner [3] extended Prandtl's work for the case of a purely frictional weightless material with the surface of the half-space loaded by a uniform surcharge and obtained a close form solution of N_q factor as follow:

$$N_q = e^{\pi \tan\phi} \tan^2\left(\frac{\pi}{4} + \frac{\phi}{2}\right) \tag{22}$$

To obtain an upper bound solution for a weightless soil with the effect of surcharge, it is convenient to consider $c = 0, q = 1, \gamma = 0$. The typical mesh is illustrated in Fig. 6. The upper bound limit analysis

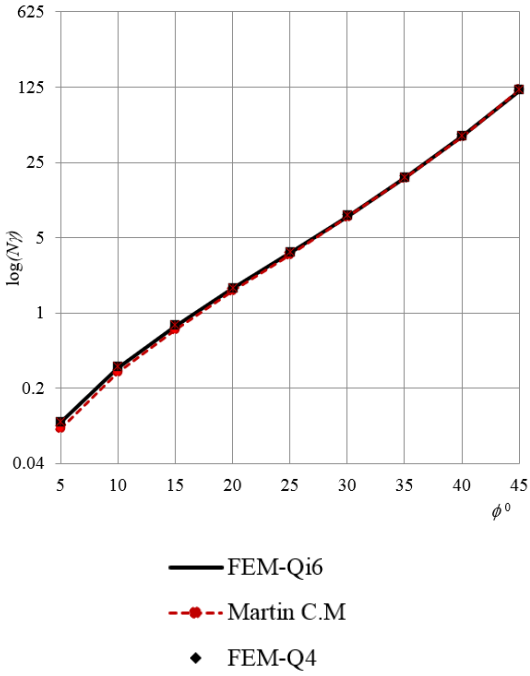

Figure 10. Comparison of N_γ factors for smooth footing

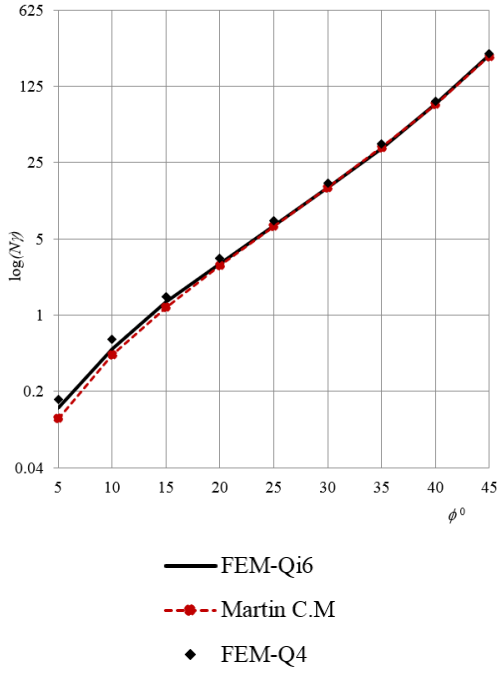

Figure 11. Comparison of N_γ factors for rough footing

problem for plane strain using FEM-Qi6 can be determined by minimizing the collapse loads.

$$N_q = \alpha^+ = \min\left(-W^0_{\text{ext}}(\dot{\mathbf{u}})\right) \tag{23}$$

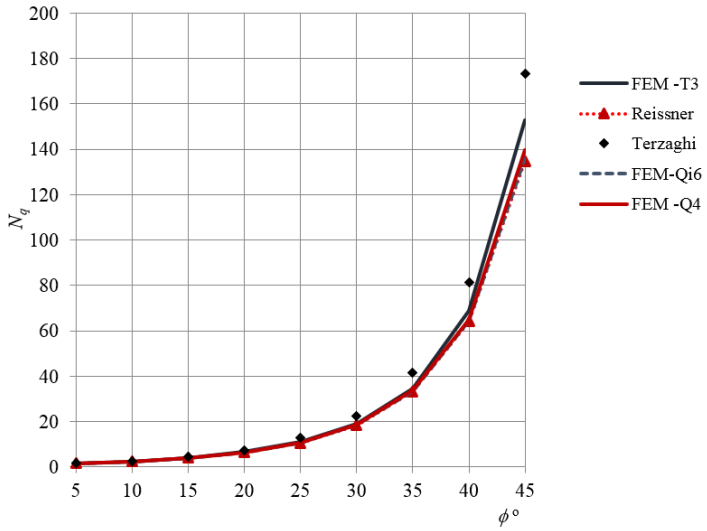

Figure 12. Comparison of N_q factors with other solutions.

The computational results of bearing capacity of strip footing N_q for friction angles $\phi = 5^\circ$ to 45° using the FEM-Qi6 approach are listed in Table 4 and shown in Fig. 12. According to the Mohr-

Coulomb yield criterion, the FEM-Qi6 results are close to the analytical solution by Reissner [3], the errors are less than 1.2%. The values of N_q using the analytical expression of Terzaghi are higher than those from the Reissner solution and other results because Terzaghi assumed an incorrect failure mechanism $\theta = \phi$.

Table 4. Results for bearing capacity factor N_q

ϕ (°)	Terzaghi [1]	FEM-T3 (Error %)	FEM-Q4 (Error %)	FEM-Qi6 (Error %)	Exact values Reissner [3]
5	1.64	1.579 (0.70)	1.579 (0.70)	1.5787 (0.68)	1.568
10	2.69	2.504 (1.33)	2.497 (1.05)	2.4968 (1.04)	2.471
15	4.45	4.013 (1.82)	3.983 (1.06)	3.9828 (1.06)	3.941
20	7.44	6.522 (1.92)	6.461 (0.97)	6.4613 (0.97)	6.399
25	12.72	11.059 (4.11)	10.748 (1.19)	10.7478 (1.18)	10.622
30	22.46	19.142 (3.93)	18.506 (0.57)	18.5062 (0.57)	18.401
35	41.44	34.569 (3.82	33.589 (0.88)	33.4094 (0.34)	33.296
40	81.27	68.612 (6.88)	64.654 (0.71)	64.5118 (0.49)	64.195
45	173.28	152.841 (13.32)	139.61 (3.51)	136.0700 (0.88)	134.874

Figs. 13–16 show the power dissipation of strip footing using NS-FEM-T3 in friction angle cases $\phi = 10°$, $20°$, $30°$ and $40°$. It is noticeable that the failure mechanism expands larger in both vertical and horizontal directions when the friction angle ϕ increase; it means that the values of N_q factors increase. Figs. 13–16 show that the NS-FEM method's failure mechanisms agree well with those from Prandtl's [2] solution.

Figure 13. Power dissipation of strip footing $\phi = 10°$

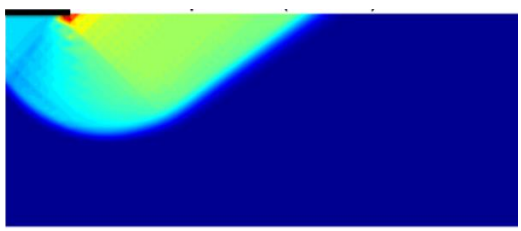

Figure 14. Power dissipation of strip footing $\phi = 20°$

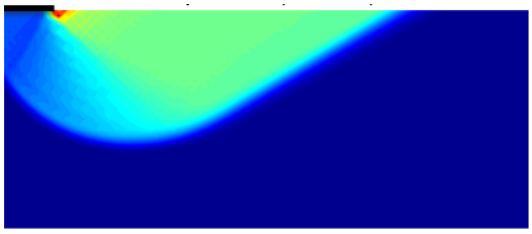

Figure 15. Power dissipation of strip footing $\phi = 30^\circ$

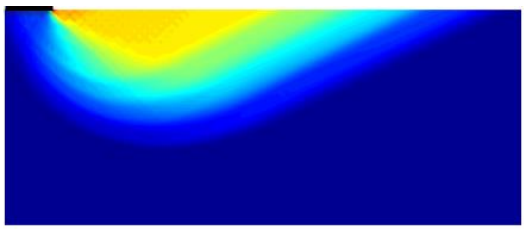

Figure 16. Power dissipation of strip footing $\phi = 40^\circ$

5. Conclusions

This paper has presented a numerical method for upper bound limit analysis to investigate the bearing capacity factors of strip footing using the enhanced-bubble function quadrilateral finite element (FEM-Qi6) and second-order cone programming (SOCP). By using the Mohr-Coulomb failure criterion and associated flow rule, the obtained results of N_c, N_q and N_γ are in perfect agreement with those results available in the literature. Therefore, FEM-Qi6 is an effective tool to evaluate the collapse load for other large problems in geomechanics.

References

[1] Terzaghi, K. (1943). *Theoretical Soil Mechanics*. New York: John Wiley & Sons.

[2] Prandtl, L. (1921). Uber die eindrigungs-festigkeit plastischer baustroffe und die festigkeit von schneiden. *Zeitschrift fur Angewandte Mathematik und Mechanik*, 1(1):15–20.

[3] Reissner, H. (1924). Zum erddruckproblem. In *Proceedings of the First International Congress for Applied Mechanics*, Delft, The Netherlands, 295–311.

[4] Meyerhof, G. G. (1963). Some recent research on the bearing capacity of foundations. *Canadian Geotechnical Journal*, 1(1):16–26.

[5] Sokolovskii, V. V. (1965). *Statics of Soil Media*. Pergamon Press.

[6] Hansen, J. B. (1970). A revised and extended formula for bearing capacity. *Bulletin of the Danish Geotechnical Institute*, 28:3–11.

[7] Vesić, A. S. (1973). Analysis of ultimate loads of shallow foundations. *Journal of the Soil Mechanics and Foundations Division*, 99(1):45–73.

[8] Caquot, A., Kérisel, J. (1953). Sur le terme de surface dans le calcul des fondations en milieu pulverulent. In *Proceedings of the Third International Conference on Soil Mechanics and Foundation Engineering*, volume 1, Zurich, 336–337.

[9] Bolton, M. D., Lau, C. K. (1993). Vertical bearing capacity factors for circular and strip footings on Mohr–Coulomb soil. *Canadian Geotechnical Journal*, 30(6):1024–1033.

[10] Griffiths, D. V. (1982). Computation of bearing capacity factors using finite elements. *Geotechnique*, 32 (3):195–202.

[11] Frydman, S., Burd, H. J. (1997). Numerical studies of bearing-capacity factor N γ. *Journal of Geotechnical and Geoenvironmental Engineering*, 123(1):20–29.

[12] Ukritchon, B., Whittle, A. J., Klangvijit, C. (2003). Calculations of bearing capacity factor N γ using numerical limit analyses. *Journal of Geotechnical and Geoenvironmental Engineering*, 129(5):468–474.

[13] Hjiaj, M., Lyamin, A. V., Sloan, S. W. (2005). Numerical limit analysis solutions for the bearing capacity factor Nγ. *International Journal of Solids and Structures*, 42(5-6):1681–1704.

[14] Martin, C. M. (2005). Exact bearing capacity calculations using the method of characteristics. In *Proceedings of the 11th International Conference of IACMAG*, Turin, 441–450.

[15] Makrodimopoulos, A., Martin, C. M. (2007). Upper bound limit analysis using simplex strain elements and second-order cone programming. *International Journal for Numerical and Analytical Methods in Geomechanics*, 31(6):835–865.

[16] Vo-Minh, T. (2020). Calculation of Bearing Capacity Factors of Strip Footing Using the Nodebased Smoothed Finite Element Method (NS-FEM). In *Geotechnics for Sustainable Infrastructure Development*, Springer, 1127–1134.

[17] Hughes, T. J. R., Cohen, M., Haroun, M. (1978). Reduced and selective integration techniques in the finite element analysis of plates. *Nuclear Engineering and design*, 46(1):203–222.

[18] Piltner, R., Taylor, R. L. (2000). Triangular finite elements with rotational degrees of freedom and enhanced strain modes. *Computers & Structures*, 75(4):361–368.

[19] Simo, J. C., Rifai, M. (1990). A class of mixed assumed strain methods and the method of incompatible modes. *International Journal for Numerical Methods in Engineering*, 29(8):1595–1638.

[20] Cardoso, R. P. R., Yoon, J. W., Mahardika, M., Choudhry, S., Alves de Sousa, R. J., Fontes Valente, R. A. (2008). Enhanced assumed strain (EAS) and assumed natural strain (ANS) methods for one-point quadrature solid-shell elements. *International Journal for Numerical Methods in Engineering*, 75(2): 156–187.

[21] Bonet, J., Burton, A. J. (1998). A simple average nodal pressure tetrahedral element for incompressible and nearly incompressible dynamic explicit applications. *Communications in Numerical Methods in Engineering*, 14(5):437–449.

[22] Phuc, H. L. H., Canh, L. V., Hung, P. D. (2020). A computational homogenization analysis of materials using the stabilized mesh-free method based on the radial basis functions. *Journal of Science and Technology in Civil Engineering (STCE) - NUCE*, 14(1):65–76.

[23] Nguyen-Xuan, H., Liu, G. R. (2013). An edge-based smoothed finite element method softened with a bubble function (bES-FEM) for solid mechanics problems. *Computers & Structures*, 128:14–30.

[24] Nguyen-Xuan, H., Liu, G. R. (2015). An edge-based finite element method (ES-FEM) with adaptive scaled-bubble functions for plane strain limit analysis. *Computer Methods in Applied Mechanics and Engineering*, 285:877–905.

[25] Vu-Hoang, T., Vo-Minh, T., Nguyen-Xuan, H. (2018). Bubble-enhanced quadrilateral finite element formulation for nonlinear analysis of geotechnical problems. *Underground Space*, 3(3):229–242.

[26] Mosek. *The MOSEK optimization toolbox for MATLAB manual*.

[27] Nagtegaal, J. C., Parks, D. M., Rice, J. R. (1974). On numerically accurate finite element solutions in the fully plastic range. *Computer Methods in Applied Mechanics and Engineering*, 4(2):153–177.

[28] César de Sá, J. M. A., Natal Jorge, R. M. (1999). New enhanced strain elements for incompressible problems. *International Journal for Numerical Methods in Engineering*, 44(2):229–248.

[29] Arnold, D. N., Brezzi, F., Fortin, M. (1984). A stable finite element for the Stokes equations. *Calcolo*, 21 (4):337–344.

[30] Matsumoto, J. (2005). A relationship between stabilized fem and bubble function element stabilization method with orthogonal basis for incompressible flows. *Journal of Applied Mechanics*, 8:233–242.

[31] Zienkiewicz, O., Taylor, R. *Finite element method: solid and fluid mechanics dynamics and non-linearity*. McGraw-Hill, New York.

[32] Neto, E. D. S., Pires, F. A., Owen, D. R. J. (2005). F-bar-based linear triangles and tetrahedra for finite strain analysis of nearly incompressible solids. Part I: formulation and benchmarking. *International Journal for Numerical Methods in Engineering*, 62(3):353–383.